



HAL
open science

Assessing Vircators' Reliability Through Uncertainty and Sensitivity Analyses Using a Surrogate Model

Mae Almansoori, Ernesto Neira, Sébastien Lalléchère, Chaouki Kasmi, Felix Vega, Fahad Alyafei

► **To cite this version:**

Mae Almansoori, Ernesto Neira, Sébastien Lalléchère, Chaouki Kasmi, Felix Vega, et al.. Assessing Vircators' Reliability Through Uncertainty and Sensitivity Analyses Using a Surrogate Model. *IEEE Access*, 2020, 8, pp.205022-205033. 10.1109/ACCESS.2020.3037347. hal-03025391

HAL Id: hal-03025391

<https://hal.science/hal-03025391>

Submitted on 26 Nov 2020

HAL is a multi-disciplinary open access archive for the deposit and dissemination of scientific research documents, whether they are published or not. The documents may come from teaching and research institutions in France or abroad, or from public or private research centers.

L'archive ouverte pluridisciplinaire **HAL**, est destinée au dépôt et à la diffusion de documents scientifiques de niveau recherche, publiés ou non, émanant des établissements d'enseignement et de recherche français ou étrangers, des laboratoires publics ou privés.

Received October 19, 2020, accepted November 8, 2020, date of publication November 11, 2020, date of current version November 20, 2020.

Digital Object Identifier 10.1109/ACCESS.2020.3037347

Assessing Vircators' Reliability Through Uncertainty and Sensitivity Analyses Using a Surrogate Model

MAE ALMANSOORI¹, (Graduate Student Member, IEEE), ERNESTO NEIRA¹, (Member, IEEE), SEBASTIEN LALLECHERE², (Member, IEEE), CHAOUKI KASMI^{1,3}, FELIX VEGA^{1,4}, (Senior Member, IEEE), AND FAHAD ALYAFEI¹

¹Directed Energy Research Centre, Technology Innovation Institute, Abu Dhabi, United Arab Emirates

²CNRS, SIGMA Clermont, Institut Pascal, Université Clermont Auvergne, 63000 Clermont-Ferrand, France

³Faculty of Electrical Engineering, Helmut Schmidt University, 22043 Hamburg, Germany

⁴Electrical Engineering Department, Universidad Nacional de Colombia—Sede Bogotá, Bogotá 111321, Colombia

Corresponding author: Mae AlMansoori (mae.almansoori@tii.ac)

ABSTRACT The performances of Vircators have been reported in different studies showing that a high discrepancy between the simulated and measured output peak power and radiating frequency can be encountered. Limited investigations have been reported where the one-variable-at-a-time methodology was applied. Performing a full analysis requires to apply statistical methods over a large number of experiments (simulation or measurement) which has been a challenge due to the computation time required to simulate Vircators. Recently, an surrogate model has been proposed to drastically reduce the computation time. In this paper, we propose to evaluate the performance variability of a Vircator considering mechanical manufacturing tolerances as well as the Pulsed Power source variability. The analysis is performed by means of well-spread stochastic methods (classical Monte Carlo, spectral techniques), and alternative sensitivity analysis approaches.

INDEX TERMS High power microwave generation, pulse power systems, statistics, uncertainty quantification.

I. INTRODUCTION

Due to their independence of external magnetic field sources and their relatively simple construction, Virtual cathode oscillators (Vircators) [1]–[4] are highly attractive. Vircators are High-Power Microwave (HPM) sources that can produce peak powers on the gigawatt range at typical frequencies from 1 GHz to 12 GHz.

The *diode* and the *drift-tube* are two adjacent regions in the Vircator that are separated by a transparent anode. The HPM generation process is initiated in the diode region when a high voltage is applied between electrodes forming plasma due to cathode material sublimating. This sublimation is a consequence of the electric field enhancement on the tip of the micro-protrusions at the cathode surface. Electrons in the plasma are accelerated by a diode electric field toward the anode, resulting in the current injection into the drift-tube

($i_b(t)$). In order to form the Virtual Cathode (VC), $i_b(t)$ must be greater than the space-charge-limiting current (I_{scl}) [5] which triggers the accumulation of the charge. The oscillation of the VC and the reflection of the electrons between the VC and the real cathode results in the HPM radiation. The complete structure of the axially extracted Vircator is shown Figure 1. The high sensitivity of the performances of the Vircator to small changes in the design variables has been reported by various authors [6]–[8]. These works have shown that the anode-cathode gap (d), the anode transparency grade (T_a) and the feed voltage (V) have a significant influence on the radiated frequency and peak power variabilities (see Figure 1). However, the majority of these works were focused on identifying the effects of the variation of a single design parameter at time [8]–[12]. This means that any potential interaction between two or more variables was not studied. Moreover, as single parameter was considered as a random variable, no clear classification of variables has been performed in terms of relevance.

The associate editor coordinating the review of this manuscript and approving it for publication was Mauro Gaggero¹.

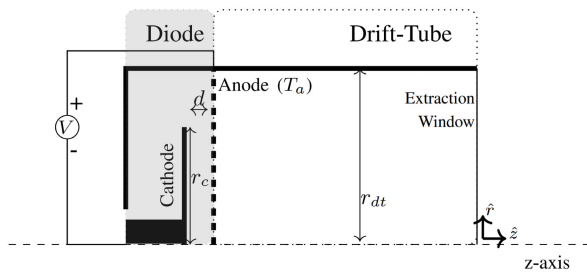


FIGURE 1. Scheme of an axially extracted Vircator. Solid of revolution view.

During the last decades, several statistical methods have been applied to electromagnetic [13]–[15], mechanical problems [16], and Vircator studies [17]–[20]. From crude Monte Carlo (MC) [21], [22] (known as a brute force technique) to Polynomial Chaos [23], [24], it has been shown how the confidence level could be assessed when dealing with random variables [25]. At the same framework, the analysis of the dominant random variables has been introduced through well-known techniques such as Morris or Sobol' indices [26]. Interesting design recommendations have been deduced as well as hardening strategies [27].

The International Standard ISO 2768-1 certification is usually applied to define the tolerances corresponding to the dimensions of machined parts. This standard specifies the general admissible ranges for the linear and angular dimensions to ensure the fabrication of the correct product. Following this standard, tolerance criteria were applied to the random variables of interest assuming linear dimensions. By having a generalised framework, the results are expected to be guideline for a wider audience due to the possibility of replicating the proposed methodology to any other mechanical structures. In addition to the mechanical variation, electrical components such as capacitors, inductors, resistors, switches as well as spark gap breakdown [28] can lead to the variation of the feed voltage waveform and coupling. Typically, the electrical components can present variations of 10 % around their nominal values. We introduce in this paper a model of the pulsed power source based on the High Current Impulse Generator (HCIG) coupled with the Vircator's Diode. This model is used as a reference in order to produce waveform similar to the previous experimentally reported results introducing components variations. Two cases are considered: a highly stable source will be considered in Case 1 and a highly varying source is proposed in Case 2. This is representative of the diversity of sources that can be found on the market.

By combining statistical methods with mechanical design tolerance and the variability of the pulsed power source, the variability of the output power (P) and the radiating frequency (f_{vc}) will be studied by considering all design inputs as Random Variables (RVs). In what follows, the variability of the peak power and the radiating frequency is evaluated,

dominant design variables are deduced from a sensitivity analysis (SA), and the interaction between RVs are estimated. Guidelines to manufacturers can be drawn in order to achieve with more certainty better performance of the Vircator.

This paper is organised as follows: in Section II, the mathematical description of the SA approach is proposed. Then, in Section III, the simulation framework used to model and simulate the Vircator is proposed. The main equations for the evaluation of the peak power and the radiating frequency are recalled. In Section IV, the SA of the studied physical quantities, namely the peak power and the radiating frequency, is described and applied considering two sets of random variables. Finally, in Section V, conclusions are drawn and design recommendations are proposed.

II. UNCERTAINTY PROPAGATION (UP) AND SENSITIVITY ANALYSIS (SA)

A. PREAMBLE

As previously pointed out, Vircators' manufacturing procedure is subject to the outcome of random processes. As a matter of fact, the tolerances and uncertainty quantification guidelines are useful to assess the effect of potential discrepancies: mechanical drifts, electrical parameters known with given margins, etc. Although, random variables are most likely associate with the resulting of random function and/or processes (so uncertain by definition), the terms random variables (RVs) in this work is referring only to, somewhat imprecisely, uncertain inputs.

Assessing the influence of uncertain variables is of utmost importance for a large diversity of complex physical scenarios [29]. In this framework, Vircator modelling and experiments require a particular care since their performance (here mainly considering the output power level P and the radiating frequency f_{vc}) are subject to uncertain behaviour.

This section will briefly define the stochastic description of a given random parameter p . Roughly considering uncertain behaviour, from a Random Variable (RV) m , one may assume:

$$m = m_0 + n \quad (1)$$

where m_0 is the statistical mean (given $m_0 \equiv E[m]$), also called the initial or mean value, and n is characterised by a given statistical distribution law having zero-mean, variance $var_n \equiv var(n)$, and Coefficient of Variation (CV) $CV_n = \sqrt{var_n}/m_0$. Thus, m and n will be defined following various statistical assumptions; for the sake of consistency regarding available information given by standards, in this example only Normal distributions will be considered, but the principles of the proposed methodology remain applicable to a variety of statistical laws (e.g. see details in [29]). Xiu [30] properly introduced the flexibility of spectral expansions for uncertainty quantification.

In the following, m may be associated to any random parameter p under evaluation such as geometrical discrepancies as well as electrical drifts. As an example, p may represent the geometrical drifts due to tolerances when manufacturing the Drift-tube (here parameter r_{dt} as given in

Figure 1). This random variations will be defined through the random variable m as depicted in equation (1). At that stage, it is important to highlight that the stochastic methodology that will be detailed hereafter will be achieved regarding a given output (see in the following Z , e.g. peak power value produced by the Vircator). Section II will give example of random parameters when dealing with Vircators' manufacturing, e.g. geometrical details: anode-cathode gap, cathode/drift-tube radii, anode transparency, electromagnetic (EM) parameters: material properties, equivalent impedance, source characteristics: feeding voltage.

Uncertainty Quantification (UQ) comprises the assessment of probabilistic and statistical outputs for two distinct classes of purposes: Uncertainty Propagation (UP) including (but not restricted to): evaluation of mean trends, probability of failures, stochastic distributions, and SA which main goal targets ranking of most influential inputs. Sensitivity analysis refers to the quantification of the robustness and accuracy of a model under certain conditions. By evaluating the influence of random variables on the fluctuation of a physical quantity (also called observable) and by evaluating the potential relationship between the random variables and the physical observable, the uncertainty of the output quantity under study can be reduced; e.g. assuming the least influential inputs to their initial values. By definition, SA aims at assessing how variations over inputs of a given model (surrogate, numerical, experimental...) affect the variability of its output(s). The Local Sensitivity Analysis (LSA) focuses on how a small perturbation in the vicinity of an input space value $m = (m^1, \dots, m^N)$ (e.g. near m where N stands for the number of inputs; four and/or eight in this work, see Tabs 6 and 9) impacts the output quantity Z (P or f_{vc} in this work). Parallel to the LSA, the input variations may be understood at a global stage (Global SA, GSA). Whether GSA may be expected from the very beginning of the system design process, it would provide useful information at a *macroscopic* stage, highlighting the most influential variables (defined with a given range of inputs). To put it in a nutshell, LSA and GSA offer complementary information: GSA gives an overview about the global response of the Vircator for a wide range of varying inputs, whereas LSA assesses the impact of small perturbation around a nominal design of inputs. In this work, and in the following, it is to be noticed only GSA has been considered through the analysis of variance techniques. The next subsection will detail the foundations of such methods.

B. ANOVA PRINCIPLES

The ANalysis Of VAriance (ANOVA) techniques are part of the GSA methods [31]. The variance-based methods rely on the evaluation of the contribution of each input parameter m^j ($j = 1, \dots, N$) to the total variance of the observable Z . Numerous works have been led in the domain of SA for a huge diversity of topics including electromagnetic and electronics [32] (design of experiment, DoE), plasma science [33] (meta-modelling for design purpose), geoscience [34] (MC).

In this context, the Russian mathematician I.M. Sobol' provided a straightforward MC-based strategy for SA of a given mapping response:

$$Z = z(m^1, m^2, \dots, m^N), \quad (2)$$

where $m = (m^1, \dots, m^N)$ is the input vector. Given a square integrable function z over an assumed integrable input space Ω^N , Sobol' considered an expansion of z into terms of increasing dimensions:

$$z = z_0 + \sum_i z_i + \sum_i \sum_{j>i} z_{ij} + \dots + z_{12\dots N}, \quad (3)$$

in which each term is square integrable over the domain of existence and is a function of the factors in its index, i.e. $z_i = z(m_i)$, $z_{ij} = z_{ij}(m^i, m^j)$. Under certain conditions, Sobol' has demonstrated from conditional expectations $E[\cdot]$ that: $z_0 = E[Z]$, $z_i = E[Z|m^i] - E[Z]$, $z_{ij} = E[Z|m^i, m^j] - z_i - z_j - E[Z]$. Finally, Sobol' proposed first-order sensitivity indices S_i since the variances of the previous term in the decomposition are the measures of importance being expected for SA:

$$S_i = \frac{\text{var}[E[Z|m^i]]}{\text{var}[Z]}, \quad (4)$$

where $E[Z|m^i]$, as aforementioned, stands for the conditional expectation given that the parameter m^i is known as the outcome of random variations. Roughly speaking, the mean of Z is evaluated assuming m^i as a random parameter.

The first-order index stands for the main effect contribution of each input factor (i in relation (4) to the variance of the observable Z). The precise assessment of such quantities (i.e. mean trends: average and variance) may be obtained at different computing costs including a large diversity of techniques [29], [35]). In the following, we will provide alternative measures (importance factors) for S_i .

C. STOCHASTIC COLLOCATION ANOVA (SCA)

Polynomial Chaos Expansion (PCE) is part of *spectral methods*; for the interested reader, some details are given in [36] dealing with PCE and stochastic collocation technique (SCT). The main idea of PCE and SCT relies on the expansion of a given random process as a linear combination of orthogonal polynomials (depending on the random inputs). Depending on the statistical assumptions (marginal probability density functions, PDFs, from the input space), a particular family of polynomials is chosen, in order to compute the most efficient representation of the random process. The governing principle consists in minimising the number of terms in the previous series for a given approximation error threshold. The fundamental principles of the SCT, when considering a given output Z and its statistical moments under N uncertain inputs m^j ($j = 1, \dots, N$), relies on its n -expansion over a Lagrangian serie. For the sake of simplicity, an illustration

for one RV may be expressed for output $Z = z(s)$ as follows:

$$z(s) = \sum_{i=1}^n Z_i L_i(s), \quad (5)$$

where $L_i(s)$ stands for the Lagrangian basis function. As pointed out in [37], a large diversity of polynomial expansions exists when dealing with stochastic surrogate modelling. In this framework, polynomial chaos expansion (PCE) and stochastic collocation techniques mainly differ by the choice of their polynomial expansion [29] (for instance Hermite polynomials). Here, Lagrange polynomials L_i were chosen (non-orthogonal polynomials but useful to simplify weight computations w_i as expressed in the following equation). Eldred *et al.* illustrated in their paper the difficulty to classify PCE and stochastic collocation, even considering the accuracy offered by Hermite polynomials when dealing with RVs normally distributed (problem dependence). It is to be noticed that this work aims at demonstrating the interest of the proposed methodology, out of any consideration regarding the rank of any given polynomial expansion to another (for instance PCE with respect to stochastic collocation technique). It is to be noticed work from [30] offers a pedagogical description of spectral techniques in the framework of uncertainty quantification, and the use of polynomial expansions.

Relying on the properties of Lagrange polynomials and assuming a PDF $p(s)$ for a given input parameter, the average of the observable Z is obtained from:

$$E[Z] = \sum_{i=1}^n w_i Z_i, \quad (6)$$

where w_i stands for the weight devoted to $Z_i = Z(s_i)$, expression of the mapping function $s \xrightarrow{\tilde{z}} Z = z(s)$ for SCT-points s_i ($i = 1, \dots, n$); and the variance of Z is given as:

$$\text{var}[Z] = \sum_{i=1}^n w_i (Z_i - E[Z])^2. \quad (7)$$

As pointed out in [29], the PCE and SCT have demonstrated their high precision and efficiency, comparatively to MC methods. However, due to the tensor product in the relations ((5)-(7)), the techniques are facing the *curse of dimensionality* that avoids an optimum use of them when increasing N for a given truncation order n . Indeed, for the sake of simplicity, the equation (5) is obtained for 1-RV case; obviously, increasing the number of RVs introduces tensor product (with respect to summation product) as evoked in [30]. In the following, we will demonstrate that the SCT offers a very high level of accuracy for variance computing with a relatively low computation costs, even when dealing with random input vector $m = (m^1, \dots, m^8)$, $N = 8$ and $n = 2$ or 3. As previously mentioned in the relation (4), the sensitivity of the RV i relatively to the other RVs is assessed through the coefficient S_i (first-order Sobol' indice). Relying on the same principle, the tensor product needed with the SCT allows straightforward assessing the same quantity from

the SCT simulations (without any extra computing costs) as follows:

$$SCA_i = \frac{\tilde{\text{var}}[Z; m^i]}{\text{var}[Z; m^1, \dots, m^N]}, \quad (8)$$

where $\tilde{\text{var}}[Z; m^i]$ represents the variance extracted considering 1-RV case m^i (i.e. considering the effect of varying RV "i" and induced Z-variance). In this work, the authors propose to take benefit from the "full-tensor" design of experiment by averaging the variance $\text{var}[Z; m^i]$ obtained using all the data points available, i.e. computing all the quantities $\text{var}[Z; m^i]$ available assuming the other RVs (out of RV "i") are set to the remaining quadrature points needed for stochastic collocation calculations. The different variances computed with the relation (7) are averaged, leading to the quantity $\tilde{\text{var}}[Z; m^i]$ (including $\tilde{\cdot}$ sign). It is to be noticed $\text{var}[Z; m^1, \dots, m^N]$ is obtained assuming the whole RV input space (i.e. with N RVs). The latter quantities are directly adapted from the relations (6) and (7). The whole methodology is called the Stochastic Collocation ANOVA (SCA).

According to the relations (4) and (8), the most influential inputs will be determined from the ranking of S_i [34] and SCA_i , being understood that the highest sensitivity indices imply the most influential parameters.

III. VIRCATOR SURROGATE MODEL

Vircator's design variables considered in this study are (see Figure 1): the Anode-cathode gap (d), the Cathode radius (r_c), the Drift-tube Radius (r_{dt}), the Anode Transparency (T_a) and the Voltage (V). In this section, the adopted frequency and power models will be described.

A. FREQUENCY MODEL

The frequency model used in this study was proposed by Alyokhin *et al.* [7] suggesting that the Vircator dominant angular frequency (ω_{vc}) can be approximated as

$$\omega_{vc} = a_1 \omega_p, \quad (9)$$

where $a_1 \approx 2.14$, and ω_p is the relativistic plasma frequency that can be expressed as [38].

$$\omega_p = \sqrt{\frac{eJ_b}{\epsilon_0 m c \sqrt{\gamma_0^2 - 1}}}, \quad (10)$$

where e and m are the electron charge and rest mass respectively, c is the speed of the light, J_b is the current density of the beam injected into the drift area, ϵ_0 is the free space permittivity and γ_0 is the relativistic factor of the electrons at the anode.

If the electron beam flow is considered laminar, Eq. (10) can be solved as a function of the design variables. To do this, J_b could be redefined as $J_d T_a$, where J_d is the diode current which can be approximated using the Child-Langmuir's [39],

[40] as

$$J_d = \frac{4}{9} \epsilon_0 \sqrt{\frac{2e}{m}} \frac{V^{3/2}}{d^2}, \quad (11)$$

where ϵ_0 is the free space permittivity.

Solving Eq. (11) and taking into account the energy conservation law, ($\gamma_0 = kV + 1$, where $k = e/mc^2$), we can transform Eq. (10) into

$$\omega_p = \frac{2^{5/4} c}{3d} \sqrt{\frac{kVT_a}{\sqrt{kV + 2}}}. \quad (12)$$

Notice that Eq. (12) is a function of the design variables and can be used directly to approximate the dominant frequency (named f_{vc} in the following, and linked to the angular frequency ω_p).

B. POWER MODEL

Regarding the Vircator's power models, there are some options available in the literature [7], [38], [41], [42]. However, the accuracy of these models is assumed under given conditions. For this study, we chose the model proposed in [38], which have been fitted from the Larmor formula [43], and simulations from XOOPIIC and XPDP1 [44]. The model defines the average power radiated at the VC frequency as:

$$\bar{P}_{\omega_p} = \frac{\pi^3 a_1^2 m}{12c^2 e} r_c^4 \omega_p^4 ((kV + 1)^2 - 1)^{3/2} \times e^{-4 \left(1 - \frac{8c^2 ((kV + 1)^{2/3} - 1)^{3/2}}{r_c^2 \omega_p^2 (1 + \ln(\frac{r_{dt}}{r_c})) \sqrt{(kV + 1)^2 - 1}} \right)^2}, \quad (13)$$

where $a_1 = 2.14$ (taken from Alyokhin's frequency model, see section III-A).

The surrogate model presented in Eq. (13) is suitable for beam currents (I_b) in the range $I_c/2 < I_b < I_c$ and $2 I_{scl} < I_b$. I_c is the critical current defining the laminar flow and can be expressed as [45]

$$I_c = k_1 \frac{r_c}{d} \sqrt{\gamma_0^2 - 1}, \quad (14)$$

and I_{scl} is the space-charge limiting current. For a solid circular beam, I_{scl} is defined as [5]:

$$I_{scl} = k_1 \frac{(\gamma_0^{2/3} - 1)^{3/2}}{1 + \ln(r_{dt}/r_b)}. \quad (15)$$

where $k_1 = 2\pi \epsilon_0 mc^3/e$.

C. DETERMINISTIC SIMULATION - MODEL VALIDATION

In this section, a deterministic simulation of a Vircator designed to operate at 7 GHz will be carried out. The geometrical variables ensuring the desired dominant frequency (according to Section III-A complying with the restrictions of the power model given in Section III-B) are provided in Table 1. The effectiveness of the surrogate model at the point of design will be validated through the comparison of numerical simulation results obtained from two different

TABLE 1. Simulation variables - deterministic simulation.

| Variables | Values |
|-----------|--------|
| V | 500 kV |
| r_{dt} | 95 mm |
| r_c | 48 mm |
| T_a | 90 % |
| d | 8.1 mm |

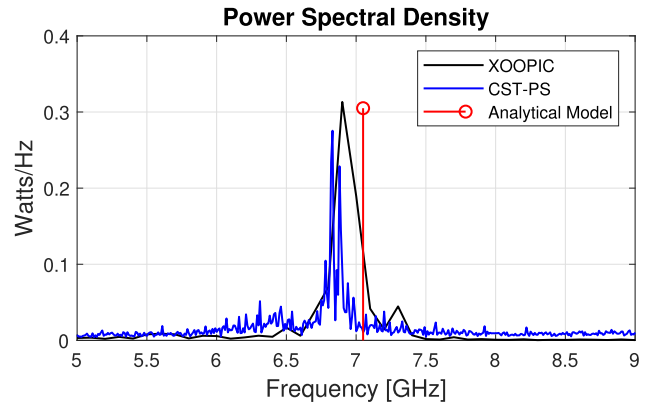


FIGURE 2. Power Spectral Density obtained by the simulation from CST-PS, XOOPIIC and the Surrogate model for Case #1.

Particle in Cell (PIC) Simulators: XOOPIIC [44] and the CST-Particles Studio.

Equations (14) and (15) can be used to calculate the values of I_c and I_{scl} as 86.2 kA and 2.2 kA respectively. For this validation, the Vircator will be fed with an ideal DC source. According to the analytical models presented in the previous section (Eqs. (12) and (13)), the dominant radiated frequency will be 7.05 GHz with a mean power of 152 MW. The model assumes no spectral dispersion (ideal simple harmonic oscillation of the VC) and non additional radiation sources, and so, the peak power results in twice the average power (ideal case). In the case of the Xoopic simulation, a 2.5D simulation was performed with 40 cells in \hat{x} and 40 cells in \hat{r} . The time of simulation was 100 ns. The power leaving the extraction window was calculated by the integration of Poynting vector (measured in each cell) over the extraction surface. The Spectral Power Density (SPD) is presented in the black line in Figure 2. The dominant frequency and peak power were 6.9 GHz and 330 MW, respectively.

For the CST simulation (3D model presented in Figure 5), the simulation was performed with 9,812,250 total number of cells and 932 emission points over the cathode surface. The total simulation time was 100 ns. The obtained SPD is presented in the blue line in Figure 2. The dominant frequency and peak power were 6.83 GHz and 279 MW, respectively. The results of the simulation and the surrogate model are summarised in Table 2. Maximum frequency error between the simulations and the model was 3.2 %. In the case of the power error, the maximum difference was between the simulation and it was of 0.73 dB.

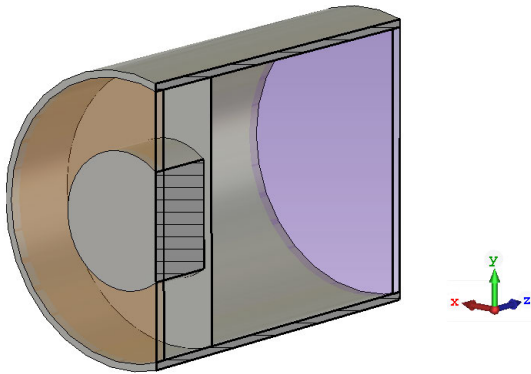


FIGURE 3. 3D model of the suggested Vircator modelled with CST.

TABLE 2. Estimated Peak Power and Radiating frequency - deterministic simulation.

| Model | Peak Power P | Radiating Frequency f_{vc} |
|-----------|----------------|------------------------------|
| CST | 273 MW | 6.83 GHz |
| XOOPIC | 330 MW | 6.9 GHz |
| Surrogate | 305 MW | 7.05 GHz |

TABLE 3. Computation power and simulation time.

| Computation SW | HW Configuration | Simulation Time |
|----------------|------------------|-----------------|
| CST | 8 (32 GB) | 67616 s |
| Xoopic | 1 (3 GB) | 790 s |
| Surrogate | 1 (3 GB) | 19 μ s |

Additionally, Table 3 presents the hardware configuration and the computation time for each simulation tools.

D. DOMAIN OF VALIDITY OF THE SURROGATE MODEL

When building a surrogate, the domain of validity remains a key evaluation step in order to perform accurate predictions. In this study, using Xoopic, a parametric analysis has been performed with regards to the following parameters. The mean error is estimated between the surrogate model and the 2.5D simulation software. Notice that the model presented in Section III-B defines the power radiated as a function of four variables V , r_c , r_{dt} , and ω_p . Where the three first are independent variables and ω_p is depending on T_a , d and V (see Eq. (12)). Tables 4 and 5 present two sets of simulations (Vircator #1 and Vircator #2) in order to evaluate the accuracy of the surrogate model. For this purpose, r_c and V vary while ω_p and r_{dt} remain constant. In order to maintain constant ω_p , the value of d was solved from Eq. (12) for a given T_a .

The first case Vircator #1, was designed with $\omega_p = 17.78 \text{ Grad/s}$, $r_{dt} = 5 \text{ cm}$ and $T_a = 50 \%$. The considered parametric variations are: linear for r_c and exponential for V . Figure 4 shows the difference between the power predicted by the surrogate model and the simulated one. The maximum error was located in point number 15 indicated with double contour line. This point is near to the minimal current ensuring the Vircator's operation (I_{scl} , see Eq. (15)). Points 2, 3, 5, 6, and 7 show errors exceeding 15dB and together, with point

TABLE 4. Simulation points, results and model predictions for the Vircator #1.

| Point | r_c [cm] | V [kV] | d [cm] | P [dBw] | | Error [dB] |
|-------|------------|----------|----------|-----------|-------|-------------|
| | | | | PIC sim | model | |
| 1 | 1 | 400 | 0.62 | 56.8 | 49.5 | 7.3 |
| 2 | 1 | 800 | 0.80 | 59.4 | -0.6 | 60 |
| 3 | 1.5 | 400 | 0.62 | 54.4 | 70.7 | 16.3 |
| 4 | 1.5 | 800 | 0.80 | 71.5 | 70.9 | 0.6 |
| 5 | 1.5 | 1600 | 0.98 | 73.5 | 57.2 | 16.3 |
| 6 | 1.5 | 3200 | 1.15 | 73.8 | 28.2 | 45.6 |
| 7 | 1.5 | 6400 | 1.29 | 76.6 | -3.6 | 80.2 |
| 8 | 2 | 400 | 0.62 | 63.9 | 73.6 | 9.7 |
| 9 | 2 | 800 | 0.80 | 70.0 | 81.6 | 11.6 |
| 10 | 2 | 1600 | 0.98 | 78.6 | 85.1 | 6.5 |
| 11 | 2.5 | 400 | 0.62 | 62.3 | 74.7 | 12.4 |
| 12 | 2.5 | 800 | 0.80 | 81.4 | 84.6 | 3.2 |
| 13 | 3 | 400 | 0.62 | 66.0 | 75.8 | 9.8 |
| 14 | 3.5 | 400 | 0.62 | 65.3 | 76.9 | 11.6 |
| 15 | 1 | 1368 | 0.94 | 70.5 | -81.5 | 152 |
| 16 | 2 | 3389 | 1.17 | 81.4 | 82.6 | 1.2 |
| 17 | 2.5 | 1712 | 1.00 | 93.0 | 93.2 | 0.2 |
| 18 | 3 | 1029 | 0.87 | 79.4 | 89.4 | 10 |
| 19 | 3.5 | 690 | 0.76 | 71.5 | 84.6 | 13.1 |

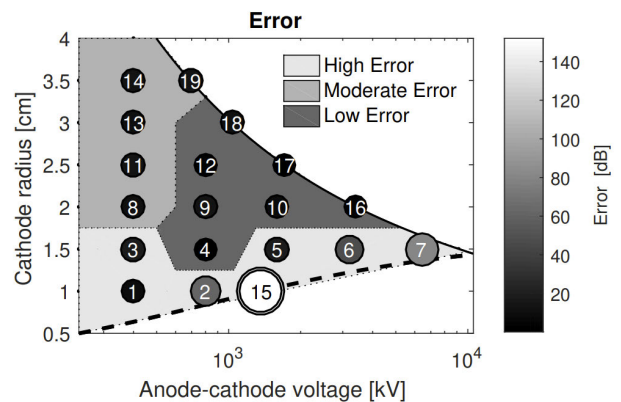


FIGURE 4. Error map between the simulated mean power and calculated using the surrogate model.

number 15, define a region where the surrogate model fails. These points are located near to the line $I_b = I_{scl}$. Points 8, 9, 11, 13, 14, and 19 exhibit errors between 5 dB and 15 dB and define a region of moderate error. Finally, the model was accurate for points 4, 12, 18, 17 and 16 which are close to the line $I_d = I_c$. Model's precision increases as the diode current tends to the critical value (I_c , see Eq. (14)). Notice that the error magnitude is represented here by colour scale and radii of the circles.

The second Vircator #2 was designed at $\omega_p = 19.50 \text{ Grad/s}$, $r_{dt} = 5 \text{ cm}$ and $T_a = 50 \%$. This example explores the whole space of variables in the same way as the previous one, but the sampling point were take on the curves determined by nI_{scl} where $n=[1 \ 2 \ 3 \ 4]$. Additionally, some samples were taken over the curve $I_c = I_d$. This sampling was defined in order to verify how the error scales over curves nI_{scl} . The maximum error was calculated for point number 9 which is on the curve I_{scl} . Notice that the points closest to this curve present significant errors. The

TABLE 5. Simulation points, results and model predictions for the Vircator #2.

| Point | r_c [cm] | V [kV] | d [cm] | P [dBW] | | Error [dB] |
|-------|------------|----------|----------|-----------|-------|-------------|
| | | | | PIC sim | model | |
| 1 | 1 | 224 | 0.46 | 44.1 | 59.4 | 15.3 |
| 2 | 1.5 | 470 | 0.62 | 65.1 | 73.1 | 8 |
| 3 | 2 | 930 | 0.58 | 85.0 | 84.4 | 0.6 |
| 4 | 1 | 291 | 0.51 | 47.4 | 60.2 | 12.8 |
| 5 | 1.5 | 725 | 0.73 | 68.4 | 75.0 | 6.6 |
| 6 | 2 | 1691 | 0.94 | 83.2 | 88.4 | 5.2 |
| 7 | 1 | 505 | 0.64 | 48.8 | 49.3 | 0.8 |
| 8 | 1.5 | 1579 | 0.93 | 67.7 | 67.3 | 0.4 |
| 9 | 1 | 1783 | 0.96 | 71.0 | -77.2 | 148.2 |
| 10 | 1.5 | 7110 | 1.24 | 83.9 | 22.5 | 65.4 |
| 11 | 2 | 2820 | 1.06 | 89.3 | 89.5 | 0.2 |
| 12 | 2.5 | 1446 | 0.9 | 94.8 | 92.4 | 0.4 |
| 13 | 3 | 884 | 0.78 | 87.6 | 84.3 | 3.3 |
| 14 | 3.5 | 597 | 0.68 | 81.7 | 79.6 | 2.1 |
| 15 | 4 | 434 | 0.6 | 73.1 | 78.5 | 5.4 |

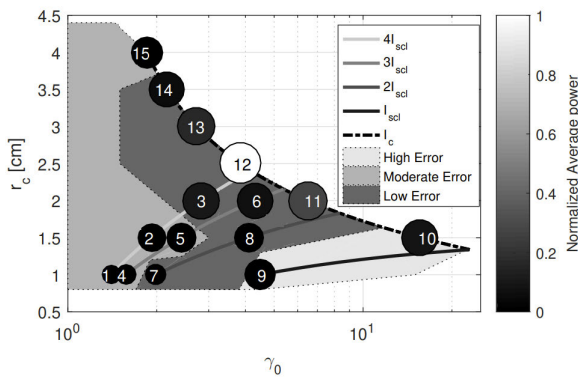


FIGURE 5. Mean power simulated for each sampled points of the Vircator #2.

model error decreases as the distance to the curve increases. In Figure 5, colours and radii, for the points simulated, do not present the error, instead it is presenting the power obtained by simulation. That figure shows that also the accuracy of the surrogate model is related to the power radiated, being better for Vircator with optimal power radiation.

The following known limitations of PIC simulations would apply:

- the plasma expansion is not considered neither in the surrogate model nor in PIC simulations;
- the plasma interaction and influence from shot-to-shot are not considered neither in the surrogate model or in PIC simulations;

Based on the evaluation of the given domain of validity of the surrogate model, we propose to perform a statistical evaluation of the peak power by introducing a set or random variables with a special care of keeping the model in the low error region (error less than 3 dB). The surrogate model, which is in good agreement with CST and XOOPIC, provides the perfect framework for an efficient statistical analysis of physical quantities for a set of given RVs.

IV. ANALYSIS OF THE VIRCATOR RESPONSE

The random geometrical variables considered in this study are proposed in Table 6. Unfortunately, no probability density functions for the Cathode radius, Drift-tube radius, Anode-

TABLE 6. Definition of Random Variables (Test case #1, see Table 1).

| RV | PDF Type | PDF Mean | PDF CV (%) |
|----------------|----------|----------|------------|
| $m^1 = r_c$ | Normal | 48 mm | 1 |
| $m^2 = r_{dt}$ | Normal | 95 mm | 1 |
| $m^3 = d$ | Normal | 8.1 mm | 10 |
| $m^4 = T_a$ | Normal | 90 % | 1 |

Cathode gap and Anode transparency are available. The tolerances have been defined based on the ISO standard for mechanical parts where the Normal distribution is recommended for the different mechanical parts with their tolerance values. Vircators are typically fed by Pulsed Power sources such as High Voltage (HVIG) or Current (HCIG) Impulse Generators which will affect the Vircator optimal operation. Two cases will be considered: first, the pulsed power source as ideal then a new set of RVs will be introduced to consider the interaction between the source and the load referred to the Vircator impedance.

A. INFLUENCE OF THE ELECTRON BEAM GENERATION

The perveance in most high power pulsed diode system is known as a time-varying increasing parameter since the electrode sheath plasma is generated which expands the anode-cathode gap distance reducing the effective gap. During the process of generating electron beam from the cathode, the electrode sheath plasma is generated. This process is highly influencing the perveance of the diode which leads to changes of the diode output characteristics. Capturing these changes in simulations tools could allow to increase the accuracy of the statistical evaluations. The first analysis proposed in the study concerns the validation of the reproduction of the perveance variability.

In recent papers published by Roy et al. [17], [19], an extensive analysis of the perveance has been proposed showing its variability due to the plasma expansion and during the shot-to-shot operation. In a Vircator vacuum diode, the 1-D solution of the current is given by the Child-Langmuir law as $I(t) = K(t)v(t)^{3/2}$, where $K(t)$ is the diode perveance and $v(t)$ is the feed voltage. For a circular cathode, the perveance can be defined as $K(t) = kr_k^2(t)/d_{ak}^2(t)$, where $k = 7.33 \times 10^{-6} V^{-3/2} A$, $r_k(t)$ is the cathode radius, and $d_{ak}(t)$ is the anode-cathode gap. Roy et al. [17], [19] have proposed an extensive experimental study of the plasma expansion and the perveance. Considering that the plasma expands radially at v_{pr} and axially at v_{px} , it has been proposed to describe the two variables as $r_k = r_o + v_{pr} \cdot t$ and $d_{ak} = d_o - v_{px} \cdot t$, with r_o being the initial emission radius and d_o the initial anode cathode gap. Defining the input parameters as random variables allows for generating different geometries using a MC simulation approach. When comparing the perveance from reported measurements/simulations [17], [19] with the stochastic surrogate model, it can be observed Fig. 6 that the variability of the perveance due to plasma expansion and

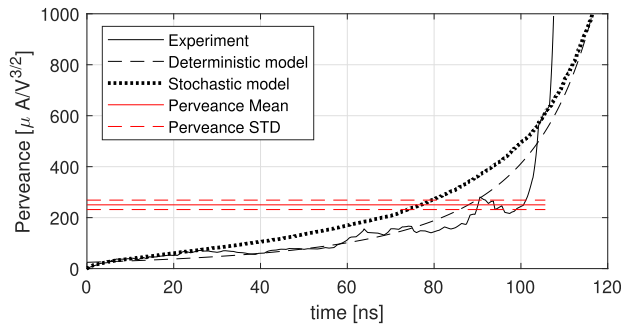


FIGURE 6. Perveance reported in [19] for a diode of $r_c = 3.5$ cm an $d_0 = 0.6$ cm constructed with velvet.

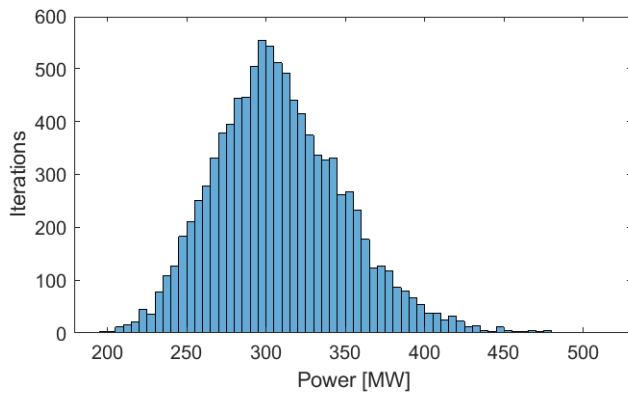


FIGURE 7. The histogram of the power computed for 10,000 random configurations taking into account mechanical variations through the 4 RVs (r_c, r_{dt}, d and T_a) of Case #1.

shot-to-shot operation are well captured by the stochastic analysis.

In what follows, the perveance will be re-computed for each random configuration in order to take into account the influence of the changes in the diode output characteristics on the peak power output.

B. TEST CASE #1: IDEAL PULSED POWER SOURCE

In this section, we are going to analyse the effects of mechanical variations only (see Table 6) which means that the feed voltage source will be considered as constant. To do that, we generated 10,000 different configurations of the Viricator varying the parameters r_c, r_{dt}, d, T_a . Note that the convergence of the 4 first statistical moments has been reached for 10,000 random configurations (less than 1 % variation on the mean, variance, skewness and kurtosis). Each Viricator was generated with a random selection of the design variables following a normal distribution, according to the PDF CV defined in Table 6. The histogram of the estimated power is presented in Figure 7. The statistical moments and the quantiles have been estimated and summarised in Table 8. It can be observed that based on descriptive statistics the output power is highly sensitive to parameters variability.

Table 7 summarises the results obtained for test Case #1 ($N = 4$ RVs) from: Sobol' indices [34] with 10,000 initial

TABLE 7. Sobol' indices (MC) and importance variables (SCA) for Test case #1 (in %), considering f_{vc} and P .

| RV | Sobol' indices S_i | | SCA $_i$ | |
|----------------|----------------------|------|----------|------|
| | f_{vc} | P | f_{vc} | P |
| $m^1 = r_c$ | 0.8 | 1.9 | 0.0 | 1.7 |
| $m^2 = r_{dt}$ | 0.8 | 0.7 | 0.0 | 0.0 |
| $m^3 = d$ | 99.7 | 98.6 | 99.8 | 98.1 |
| $m^4 = T_a$ | 1.0 | 0.9 | 0.3 | 0.3 |

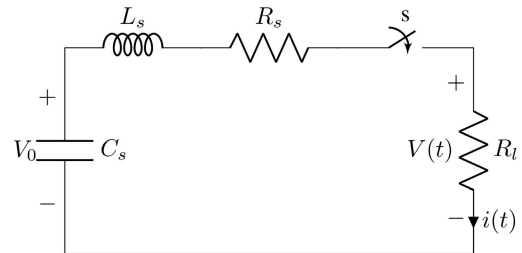


FIGURE 8. HCIG schematic.

population, SCA considering SCT $n - expansion$ ($n = 2$), leading to $2^N = 2^4 = 16$ simulations and $3^N = 3^4 = 81$ (data not shown here). Results shows the excellent agreement between Sobol' indexes and SCA importance variables, highlighting the prominent impact of d -parameter (in comparison to other random inputs) when dealing with f_{vc} -output. By repeating Sobol' analysis from 10,000 realisations of random procedure, same conclusions are obtained focusing on P -observable (see Table 7. It is to be noticed that SCA offers excellent agreement with respect to Sobol' indices (at the same time considering P and f_{vc} outputs, without any extra computing costs, meaning respectively 16 and 81 SCT simulations). Although the SCT expansion number is bounded here ($n = 2$ and 3), the convergence level is extremely high (data not shown here), jointly with very accurate data.

C. Test CASE #2: NON-IDEAL PULSED POWER SOURCE

Figure 8 presents the typical HCIG schematic, which is a serial circuit formed by a capacitance C_s charged at V_0 at $t \leq 0$, an inductance L_s , and internal resistance R_s , a switch S and a impedance R_l representing the load (i.e Viricator). Note that the switch S is considered ideal in the present analysis. The differential equation defining the circuit could be written as [46]

$$i(t)'' + ai(t)' + bi(t) = 0, \tag{16}$$

with initial conditions

$$i(0)' = V_0/L_s, \quad i(0) = 0. \tag{17}$$

In the Viricator diode region, the plasma covering cathode surface expands in the time leading to the variation of the cathode radius and the anode-cathode gap. If these effects are not considered, we can define

$$a = \frac{1}{L_s} (R_s + R_l), \tag{18}$$

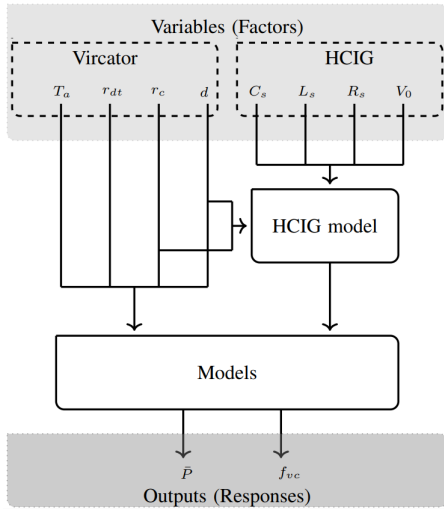


FIGURE 9. Block diagram of the uncertainty propagation for Case #2.

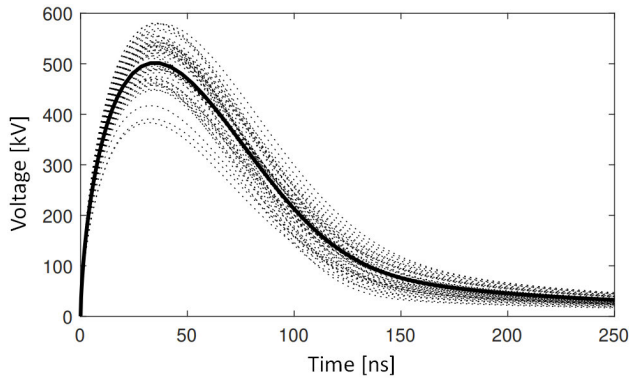


FIGURE 10. The voltage waveform; solid line is the mean value of the source, the dotted lines are random configurations.

and

$$b = \frac{1}{L_s} \left(\frac{1}{C_s} + \frac{d}{dt} R_l \right), \quad (19)$$

Additionally, the current in a vacuum diode can be defined as [47] (see Eq. (11))

$$i(t) = Kv(t)^{3/2}, \quad (20)$$

where K is the perveance.

R_l can be defined, from Eq. (20), as

$$R_l = \frac{v(t)}{i(t)} = \frac{1}{K^{2/3} i(t)^{1/3}}, \quad (21)$$

For circular cathodes, K could be stated as

$$K = \frac{4\pi}{9} \epsilon_0 \sqrt{\frac{2e}{m}} \frac{r_c^2}{d^2}. \quad (22)$$

The solution for the set of equation stated from Eqs. (16) to (22) can be obtained by numerical means.

This HCIG model introduces four new variables (L_s , C_s , V_0 and R_s). The number of realizations needed was $2^8 =$

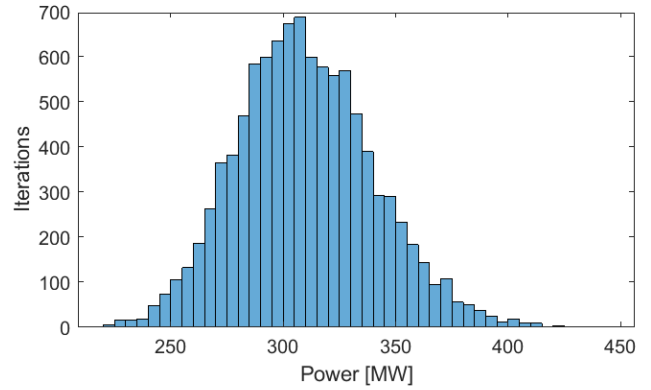


FIGURE 11. The histogram of the power generated for 10,000 random configurations taking into account mechanical and electrical variations through 8 RVs (r_c , r_{dt} , d , T_a , R_s , C_s , L_s , and V_0) for case #2.

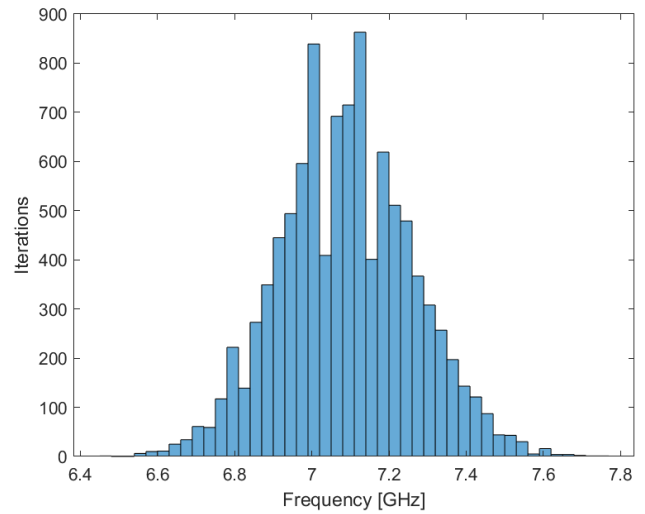


FIGURE 12. The histogram of the frequency generated for 10,000 random configurations taking into account mechanical and electrical variations through 8 RVs (r_c , r_{dt} , d , T_a , R_s , C_s , L_s , and V_0) for case #2.

TABLE 8. Statistical analysis of the peak power and radiating frequency for case #1 and #2.

| Parameter | Power (#1,#2) | Frequ. (#1,#2) |
|--------------|--------------------|------------------|
| Mean | 308.6, 309.8 [MW] | 7.07, 7.09 [GHz] |
| STD | 40.8, 30.5 [MW] | 0.23, 0.17 [GHz] |
| Quantile 0.1 | 258.2, 271.95 [MW] | 6.78, 6.87 [GHz] |
| Quantile 0.9 | 361.7, 349.71 [MW] | 7.37, 7.31 [GHz] |
| Skewness | 0.452, 0.295 | 0.176, 0.09 |
| Kurtosis | 3.393, 3.160 | 3.012, 2.972 |

256 and 10, 000, respectively for SCA and MC-like Sobol' indices. Figure 9 present the general schematic of the problem. Notice that now the problem presents eight design variables. The values of $V_0 = 1480$ kV, $R_s = 3 \Omega$, $L_s = 200$ nH, and $C_s = 5$ nF were chosen to produce a peak power of 500 kV for the central mechanical design of the Vircator (see Figure 10, solid back line). Table 9 shows the typical variation of the elements. Figure 10 presents the waveform of 50 random configurations of the source. Peak

TABLE 9. Definition of Random Variables, including PP Source (Test case #2 relying on variables from Test case #1).

| RV | PDF Type | PDF Mean | PDF CV (%) |
|-------|----------|----------------|------------|
| R_s | Normal | 3 [Ω] | 10 |
| C_s | Normal | 5 [nF] | 10 |
| L_s | Normal | .2 [μH] | 5 |
| V_0 | Normal | 1480 [kV] | 10 |

TABLE 10. Sobol' indices (MC) and importance parameters (SCA) for Test case #2 (in %), considering f_{vc} and P .

| RV | Sobol' indices S_i | | SCA _i | |
|----------------|----------------------|------|------------------|------|
| | f_{vc} | P | f_{vc} | P |
| $m^1 = R_s$ | 1.1 | 3.4 | 0.5 | 2.7 |
| $m^2 = C_s$ | 1.0 | 3.1 | 0.8 | 3.4 |
| $m^3 = L$ | 1.6 | 1.3 | 0.2 | 0.9 |
| $m^4 = V_0$ | 18.0 | 90.0 | 20.0 | 90.0 |
| $m^5 = r_c$ | 1.6 | 0.7 | 0.3 | 0.0 |
| $m^6 = r_{dt}$ | 1.7 | 0.7 | 0.0 | 0.0 |
| $m^7 = d$ | 78.2 | 4.0 | 77.6 | 3.7 |
| $m^8 = Ta$ | 1.3 | 0.8 | 0.5 | 0.2 |

voltage variation is in good agreement with experimental results [19]. As in the case of the ideal source, we performed 10,000 evaluations of different random variation of the design variables. The histograms of the estimated peak powers and operating frequencies are provided in Figure 11 and Figure 12 respectively. Descriptive statistics are summarised in Table 8. Table 10 synthesises the sensitivity analysis achieved for Test case #2 (8 RVs) considering the radiating frequency f_{vc} and the power P . Complementary to Test case #1, the d -parameter remains the most influential one with f_{vc} -output; in this framework, it is to be noticed that the voltage V_0 plays an important role. The results obtained from Sobol' indices and SCT importance variables agree very well. As expected, introducing non-ideal voltage source involves extra influence of the voltage parameter (here V_0) with differences depending on the considered output: for f_{vc} (Table 10, SA leads to ranking the most influential parameter as follows: respectively d - and V_0 -input, regarding P (Table 10, the uncertain variations around V_0 -parameter are the most influential ones, far from d -input (less influential than in previous case). Out of d and V_0 , through a first-order analysis, the other inputs may be assumed as constant parameters. These results are in concordance with previous experimental studies available in the literature [8]–[12].

V. CONCLUSION

A stochastic analysis based on the surrogate model of the Vircator has been proposed with a focus on general tendencies (i.e mean and variance analysis) of physical quantities based on Sobol' indices and SCA. The influence of mechanical tolerances and electrical source variability on the performance of Virtual cathode oscillators has been evaluated. Two cases were analysed. Case #1 took into account the mechanical parameters only; whereas for Case #2, the effects of the non-ideal pulsed power source was considered as well.

The anode-cathode gap (d) was found to be the parameter with the highest impact on the power and the frequency in the case of the ideal source. This high significance could be a consequence of the high percentage of variability due to its cumbersome fixing. In the non-ideal pulsed power source case, Voltage (V) is the most significant parameter for the power, while d has the highest impact on the frequency. The results obtained in this study validated the experimental reports that have suggested the high dependency of the Vircator's outputs on the feed Voltage (V) and anode-cathode gap d . It is to be noted that the proposed strategy, including surrogate Vircator's modelling, provides an efficient methodology to assess realistic statistical information regarding the Vircator's behaviour. Furthermore, as an alternative to brute force Sobol' design methodology, SCA offers trustworthy guidelines to minimise the random variations due to mechanical manufacturing, at reduced computing costs (hundreds of simulations at maximum). The proposed framework can easily be adapted in terms of number of random variables and distributions. This would allow other research groups to evaluate the influence of different random assumptions, e.g. uncertainties introduced by manufacturers tolerances, electronic components variability through the definition of coefficients of variation and probability density functions.

ACKNOWLEDGMENT

The authors would like to thank Dr. Juan Coronel from the Directed Energy Research Centre, Technology Innovation Institute, for his recommendations on the proposed study.

REFERENCES

- [1] A. N. Didenko, A. G. Zherlitsyn, and G. V. Melnikov, "Research of microwave generation efficiency for triode with virtual cathode (vircator triode)," in *Proc. 12th Int. Conf. High-Power Part. Beams (BEAMS)*, vol. 1, Jun. 1998, pp. 65–68. [Online]. Available: <http://ieeexplore.ieee.org/lpdocs/epic03/wrapper.htm?arnumber=822391>
- [2] A. E. Dubinov, I. A. Efimova, I. Y. Kornilova, S. K. Saikov, V. D. Selemir, and V. P. Tarakanov, "Nonlinear dynamics of electron beams with a virtual cathode," *Phys. Particles Nuclei*, vol. 35, no. 2, p. 251–284, 2004.
- [3] D. J. Sullivan, "High power microwave generation from a virtual cathode oscillator (vircator)," *IEEE Trans. Nucl. Sci.*, vol. 30, no. 4, pp. 3426–3428, Aug. 1983.
- [4] R. Mahaffey, "High-power microwaves from a non-isochronic reflexing system," *Phys. Rev. Lett.*, vol. 39, p. 843, Sep. 1977.
- [5] J. Benford, J. Swegle, and E. Schamiloglu, *High Power Microwaves* (Series in Plasma Physics). Boca Raton, FL, USA: CRC Press, 2007. [Online]. Available: <https://books.google.ae/books?id=qHCPPQvr12sC>
- [6] G. Singh and S. Chaturvedi, "PIC simulation of effect of energy-dependent foil transparency in an axially-extracted vircator," *IEEE Trans. Plasma Sci.*, vol. 32, no. 6, pp. 2210–2216, Dec. 2004.
- [7] B. V. Alyokhin, A. E. Dubinov, V. D. Selemir, O. A. Shamro, K. V. Shibalko, N. V. Stepanov, and V. E. Vatrunin, "Theoretical and experimental studies of virtual cathode microwave devices," *IEEE Trans. Plasma Sci.*, vol. 22, no. 5, pp. 945–959, Oct. 1994.
- [8] M. C. Choi, S. H. Choi, M. W. Jung, K. K. Seo, Y. H. Seo, K. S. Cho, E. H. Choi, and H. S. Uhm, "Characteristic of vircator output at various AK gap distances with diode pervance," in *Proc. IEEE Conf. Rec. Pulsed Power Plasma Sci., 28th IEEE Int. Conf. Plasma Sci., 13th IEEE Int. Pulsed Power Conf. (PPPS)*, Jun. 2001, p. 503.

- [9] C.-S. Hwang and M.-W. Wu, "A high power microwave vircator with an enhanced efficiency," *IEEE Trans. Plasma Sci.*, vol. 21, no. 2, pp. 239–242, Apr. 1993.
- [10] R. Verma, R. Shukla, S. K. Sharma, P. Banerjee, R. Das, P. Deb, T. Prabaharan, B. Das, E. Mishra, B. Adhikary, K. Sagar, M. Meena, and A. Shyam, "Characterization of high power microwave radiation by an axially extracted vircator," *IEEE Trans. Electron Devices*, vol. 61, no. 1, pp. 141–146, Jan. 2014.
- [11] V. Baryshevsky, A. Gurinovich, E. Gurnevich, and P. Molchanov, "Experimental study of a triode reflex geometry vircator," *IEEE Trans. Plasma Sci.*, vol. 45, no. 4, pp. 631–635, Apr. 2017.
- [12] L. Li, L. Liu, G. Cheng, Q. Xu, H. Wan, L. Chang, and J. Wen, "The dependence of vircator oscillation mode on cathode material," *J. Appl. Phys.*, vol. 105, no. 12, Jun. 2009, Art. no. 123301, doi: 10.1063/1.3151863.
- [13] Y. Wang and W. Xu, "Probability statistical method of assisting electromagnetic compatibility index decision-making," in *Proc. IEEE Int. Symp. Electromagn. Compat. IEEE Asia-Pacific Symp. Electromagn. Compat. (EMC/APEMC)*, May 2018, pp. 509–512.
- [14] Z. Yuan, Z. Xiang, Y. Liping, Z. Haijing, and H. Kama, "High frequency response sensitivity of electrically large enclosure with aperture and its statistical analysis method," in *Proc. Asia-Pacific Symp. Electromagn. Compat. (APEMC)*, May 2015, pp. 185–188.
- [15] T. Liang, G. Spadacini, F. Grassi, and S. A. Pignari, "Coupling of wideband radiated IEMI to wiring harness: A statistical analysis of the main influencing parameters," in *Proc. IEEE Symp. Electromagn. Compat., Signal Integrity Power Integrity (EMC, SI PI)*, Jul. 2018, pp. 357–362.
- [16] I. Saleem, M. Aslam, and M. Azam, "The use of statistical methods in mechanical engineering," *Res. J. Appl. Sci., Eng. Technol.*, vol. 5, no. 7, pp. 2327–2331, Mar. 2013.
- [17] A. Roy, R. Menon, S. K. Singh, M. R. Kulkarni, P. C. Saroj, K. V. Nagesh, K. C. Mittal, and D. P. Chakravarty, "Shot to shot variation in perveance of the explosive emission electron beam diode," *Phys. Plasmas*, vol. 16, no. 3, Mar. 2009, Art. no. 033113, doi: 10.1063/1.3097903.
- [18] A. Roy, A. Sharma, V. Sharma, A. Patel, and D. P. Chakravarty, "Frequency variation of a reflex-triode virtual cathode oscillator," *IEEE Trans. Plasma Sci.*, vol. 41, no. 1, pp. 238–242, Jan. 2013.
- [19] A. Roy, R. Menon, K. V. Nagesh, and D. P. Chakravarty, "High-current density electron beam generation from a polymer velvet cathode," *J. Phys. D, Appl. Phys.*, vol. 43, no. 36, Aug. 2010, Art. no. 365202.
- [20] A. Roy, S. K. Singh, R. Menon, D. Senthil Kumar, S. Khandekar, V. B. Somu, S. Chottray, P. C. Saroj, K. V. Nagesh, K. C. Mittal, and D. P. Chakravarty, "Pulsewidth variation of an axial vircator," *IEEE Trans. Plasma Sci.*, vol. 38, no. 7, pp. 1538–1545, Jul. 2010.
- [21] P. Naenna and J. T. Johnson, "Monte Carlo simulation of altimeter pulse returns and electromagnetic bias," in *Proc. IEEE Int. Geosci. Remote Sens. Symp. (IGARSS)*, vol. 5, Jul. 2008, pp. 120–123.
- [22] A. De Leo, V. M. Primiani, P. Russo, and G. Cerri, "Numerical analysis of a reverberation chamber: Comparison between mechanical and source stirring techniques," in *Proc. Int. Symp. Electromagn. Compat. (EMC Eur.)*, Sep. 2017, pp. 1–6.
- [23] H. Acikgoz and R. Mittra, "Statistical analysis of electromagnetic structures and antennas using the polynomial chaos expansion method," in *Proc. 11th Eur. Conf. Antennas Propag. (EUCAP)*, Mar. 2017, pp. 798–800.
- [24] R. Mittra, Ed., *Developments in Antenna Analysis and Design* (Electromagnetic Waves), vol. 2. Edison, NJ, USA: IET, 2018. [Online]. Available: <https://digital-library.theiet.org/content/books/ew/sbaw543g>
- [25] T. Houret, P. Besnier, S. Vauchamp, and P. Pouliguen, "Estimating the probability density function of the electromagnetic susceptibility from a small sample of equipment," *Prog. Electromagn. Res. B*, vol. 83, pp. 93–109, Mar. 2019.
- [26] O. Yuzugullu, S. Marelli, E. Erten, B. Sudret, and I. Hajnsek, "Global sensitivity analysis of a morphology based electromagnetic scattering model," in *Proc. IEEE Int. Geosci. Remote Sens. Symp. (IGARSS)*, Jul. 2015, pp. 2743–2746.
- [27] E. Burnaev, I. Panin, and B. Sudret, "Efficient design of experiments for sensitivity analysis based on polynomial chaos expansions," *Ann. Math. Artif. Intell.*, vol. 81, pp. 187–207, Mar. 2017.
- [28] A. A. Razi Kazemi and K. Niayesh, "Impact of spark gap breakdown phenomena on the output voltage of compact Marx generators," *IEEE Trans. Dielectr. Electr. Insul.*, vol. 18, no. 4, pp. 1022–1028, Aug. 2011.
- [29] S. Lallechere, C. F. M. Carobbi, and L. R. Arnaud, "Review of uncertainty quantification of measurement and computational modeling in EMC part II: Computational uncertainty," *IEEE Trans. Electromagn. Compat.*, vol. 61, no. 6, pp. 1699–1706, Dec. 2019.
- [30] D. Xiu, "Fast numerical methods for stochastic computations: A review," *Commun. Comput. Phys.*, vol. 5, nos. 2–4, pp. 242–272, 2009.
- [31] B. Iooss and P. Lemaitre, "Uncertainty management in simulation-optimization of complex systems—Algorithms and applications," in *A Review on Global Sensitivity Analysis Methods*. Boston, MA, USA: Springer, 2015, pp. 101–122.
- [32] M. Breant, O. Maurice, G. Duchamp, and T. Dubois, "To improve the variability of one complex system with the MKME," in *Proc. Int. Symp. Electromagn. Compat. (EMC Eur.)*, Roma, Italy, Sep. 2012, pp. 1–6.
- [33] C. H. Noh, W. Chung, J. Lim, and B. C. Lee, "Design optimization of the interim support of the ITER lower cryostat thermal shield using a metamodel," *IEEE Trans. Plasma Sci.*, vol. 44, no. 9, pp. 1684–1688, Sep. 2016.
- [34] F. Cannavò, "Sensitivity analysis for volcanic source modeling quality assessment and model selection," *Comput. Geosci.*, vol. 44, pp. 52–59, Jul. 2012.
- [35] Z. Fei, Y. Huang, J. Zhou, and C. Song, "Numerical analysis of a transmission line illuminated by a random plane-wave field using stochastic reduced order models," *IEEE Access*, vol. 5, pp. 8741–8751, 2017.
- [36] T. E. Lovett, F. Ponci, and A. Monti, "A polynomial chaos approach to measurement uncertainty," *IEEE Trans. Instrum. Meas.*, vol. 55, no. 3, pp. 729–736, Jun. 2006.
- [37] M. Eldred and J. Burkardt, "Comparison of non-intrusive polynomial chaos and stochastic collocation methods for uncertainty quantification," in *Proc. AIAA*, vols. 0976–2009, 2009, pp. 1–20.
- [38] E. Neira, Y.-Z. Xie, and F. Vega, "On the virtual cathode oscillator's energy optimization," *AIP Adv.*, vol. 8, no. 12, Dec. 2018, Art. no. 125210, doi: 10.1063/1.5045587.
- [39] I. Langmuir, "The effect of space charge and residual gases on thermionic currents in high vacuum," *Phys. Rev.*, vol. 2, no. 6, pp. 450–486, Dec. 1913. [Online]. Available: <http://link.aps.org/doi/10.1103/PhysRev.2.450>
- [40] C. D. Child, "Discharge from hot cao," *Phys. Rev. I*, vol. 32, no. 5, pp. 492–511, May 1911. [Online]. Available: <http://link.aps.org/doi/10.1103/PhysRevSeriesI.32.492>
- [41] J. I. Katz, "Dimensional bounds on vircator emission," *IEEE Trans. Plasma Sci.*, vol. 44, no. 12, pp. 3268–3270, Dec. 2016.
- [42] D. Biswas, "A one-dimensional basic oscillator model of the vircator," *Phys. Plasmas*, vol. 16, no. 6, Jun. 2009, Art. no. 063104.
- [43] M. A. Heald and J. B. Marion, *Classical Electromagnetic Radiation*, 3rd ed. Thousand Oaks, CA, USA: Thomson Learning, 1995.
- [44] J. P. Verboncoeur, M. V. Alves, V. Vahedi, and C. K. Birdsall, "Simultaneous potential and circuit solution for 1D bounded plasma particle simulation codes," *Comput. Phys.*, vol. 104, no. 2, pp. 321–328, 1993.
- [45] S. Putnam, *Theoretical Studies of Intense Relativistic Electron Beam-Plasma Interactions*, 1st ed. San Leandro, CA, US: Physics International Company, 1972.
- [46] E. Kuffel, W. Zaengl, and J. Kuffel, *High Voltage Engineering Fundamentals*, 2nd ed. E. Kuffel, W. Zaengl, and J. Kuffel, Eds. Oxford, U.K.: Newnes, 2000, pp. 1–7. [Online]. Available: <http://www.sciencedirect.com/science/article/pii/B9780750636346500022>
- [47] M. C. Choi, S. H. Choi, K. B. Song, Y. Jung, T. S. Cho, Y. Seo, G. S. Cho, and E. H. Choi, "Characteristics of diode perveance and vircator output under various anode-cathode (A-K) gap distances," in *Pulsed Power Plasma Sci., 28th IEEE Int. Conf. Plasma Sci., 13th IEEE Int. Pulsed Power Conf. Dig. Papers (PPPS)*, vol. 2, Jun. 2001, pp. 1649–1652.



MAE ALMANSOORI (Graduate Student Member, IEEE) received the M.Sc. degree in mechanical engineering from Khalifa University, Abu Dhabi, United Arab Emirates, in 2019.

She served as a Researcher for the Aerospace Research and Innovation Center, focusing on structural designing. She is currently working as a Senior Mechanical Researcher with the Directed Energy Research Centre, Technology Innovation Institute, Abu Dhabi, applying state-of-the-art

mechanical engineering processes to high power electromagnetic sources. Her research interests include structural designing, materials and mechanical analysis, additive manufacturing, and heat exchangers. She is currently working on switched oscillators and high power microwave systems such as the Viricator focusing on optimization problems using statistical methods. Furthermore, she is developing her knowledge in the current electromagnetic accelerator (Railgun) project at the Directed Energy Research Centre. In 2020, she received the "Young Scientist Award" from the International Union of Radio Science (URSI)—German Section during Kleinheubacher Tagung.



CHAOUKI KASMI received the double master's degrees in embedded electronics from ESEO, Angers, France, and in microelectronics from Institut National des Sciences Appliquées de Rennes, Rennes, France, in 2009, and the Ph.D. degree in electronics from Sorbonne University—Paris VI, France.

In 2009, he joined the Wireless Security Laboratory, French Network and Information Security Agency, Paris, as a Researcher in Electromagnetic

Security. He is currently the Chief Research Officer of the Directed Energy Research Centre, Technology Innovation Institute, Abu Dhabi, United Arab Emirates, and an Associate Scientist with the Faculty of Electrical Engineering, Helmut Schmidt University, Hamburg, Germany. He also serves as the Vice-President of Commission E for the International Union of Radio Science (URSI), France, and Early Career Representative at International level. His research interests include electromagnetic interferences, including propagation, complex EM environments, statistical electromagnetics, and cyber electromagnetics. He received the Young Scientist Award from URSI, in 2014 and 2015, and has been given a HPEM Life Fellow from the SUMMA Foundation.



ERNESTO NEIRA (Member, IEEE) was born in Cachipay, Cundinamarca, Colombia, in 1981. He received the B.S. degree in electronic engineering from the Universidad Distrital Francisco José de Caldas, Bogotá, Colombia, in 2005, and the Ph.D. degree in engineering from the Universidad Nacional de Colombia, Bogotá, in 2019.

From 2008 to 2013, he was a Researcher with the Universidad Nacional de Colombia, in the topic of landmines and explosives with a grant

from Colombian Army. He is currently working with the Directed Energy Research Centre, Technology Innovation Institute, Abu Dhabi, United Arab Emirates. His research interests include high power microwaves, electromagnetic compatibility, and telecommunications.

Mr. Neira is the winner of the Engineering Award Enrique Morales 2011 by the Sociedad Colombiana de Ingenieros and the Scientist Award from the Francisco José de Caldas 2012 granted by the Group of Ingenieros Militares of Colombia for important contributions in the solution of the problematic of the Colombian landmines.



FELIX VEGA (Senior Member, IEEE) received the Ph.D. degree in electrical engineering from the Swiss Federal Institute of Technology Lausanne (EPFL), Switzerland, and the second Ph.D. degree in electrical engineering from the National University of Colombia.

He is the Director of Electromagnetic Research and Development at the Directed Energy Research Centre, a Centre affiliated with the Technology Innovation Institute (TII), Abu Dhabi, United Arab

Emirates. He is also a Professor of Antennas and Electromagnetism with the Universidad Nacional de Colombia, Bogotá. His research interests include high power electromagnetic sources, antennas, and effects on systems. He is a HPEM Fellow of the SUMMA Foundation. He received the "Young Scientist Award" from URSI, in August 2008, the "Frank Gunther Award" from the Radio Club of America, in 2011, the Best Applied Paper Award from the SUMMA Foundation series of Notes 2010–2012, in 2012, and the "John Howard Memorial Award" from the IEEE—EMC Society, in 2015. He is the Secretary of the IEEE Antennas and Propagation Society.



SEBASTIEN LALLECHERE (Member, IEEE) received the Ph.D. degree in electronics/electromagnetics from Université Blaise Pascal, Clermont-Ferrand, France, in 2006, and the French "Habilitation à Diriger des Recherches" (HDR) in electronics/electromagnetics from Université Clermont Auvergne (UCA), Clermont-Ferrand, in 2018.

He served as a Research Engineer with the LASMEA, Clermont-Ferrand, in 2007, focusing on intensive computational methods for electromagnetics. He is currently an Associate Professor with the Institut Pascal, UCA. His research interests include the fields of electromagnetic compatibility, including antennas and propagation, complex electromagnetic environments, computational electromagnetics, and stochastic modeling in electrical engineering.



FAHAD ALYAFEI received the B.Sc. degree in electrical engineering from Virginia Commonwealth University, USA, the M.B.A. degree from the American University in Dubai, the master's (Diploma) degree in electricity supply management from Cambridge University, U.K., and the Ph.D. degree in transfer of technology from Brunel University London, in 2013. He was an Advisor in Business Development with Tawazun Economic Council. He worked for almost 20 years in the

leading positions at prominent organizations both inside and outside the UAE, including the Emirates Identity Authority, Abu Dhabi Distribution Company, Abu Dhabi Water & Electricity Authority, Thuraya Satellite Telecommunications Company, and Virginia Microelectronic Center, Richmond, VA, USA.

...